

ORIGINAL ARTICLE

Quasi noise-free digital holography

Vittorio Bianco¹, Pasquale Memmolo¹, Melania Paturzo¹, Andrea Finizio¹, Bahram Javidi² and Pietro Ferraro¹

One of the main drawbacks of Digital Holography (DH) is the coherent nature of the light source, which severely corrupts the quality of holographic reconstructions. Although numerous techniques to reduce noise in DH have provided good results, holographic noise suppression remains a challenging task. We propose a novel framework that combines the concepts of encoding multiple uncorrelated digital holograms, block grouping and collaborative filtering to achieve quasi noise-free DH reconstructions. The optimized joint action of these different image-denoising methods permits the removal of up to 98% of the noise while preserving the image contrast. The resulting quality of the hologram reconstructions is comparable to the quality achievable with non-coherent techniques and far beyond the current state of art in DH. Experimental validation is provided for both single-wavelength and multi-wavelength DH, and a comparison with the most used holographic denoising methods is performed.

Light: Science & Applications (2016) **5**, e16142; doi:10.1038/lsa.2016.142; published online 9 September 2016

Keywords: coherent noise reduction; digital holography; image reconstruction techniques; multiplex holography; noise in imaging systems; speckle

INTRODUCTION

Digital Holography (DH) is a powerful imaging technique to record and display the 3D information content of an object^{1,2}. DH has led to the development of a huge set of applications in many fields, including quantitative label-free microscopy of transparent samples in biology and medicine^{3–5}, on-chip holographic microscopy for point-of-care diagnostics^{6–8}, holographic displays for entertainment^{9–12}, non-destructive testing for industrial applications¹³, cryptography¹⁴ and homeland security^{15,16}. Recently, DH has taken a huge step toward recording and displaying large-size real-world objects employing far-infrared illumination¹⁵ (IRDH). However, due to the coherent nature of the laser sources, digital holograms are corrupted by a mixture of coherent speckle and incoherent additive noise, which can severely degrade the reconstruction quality and/or the optical display. Moreover, such mixtures are hard to model statistically¹⁷.

Currently, the most intuitive way to address this problem is to reduce the light coherence by engineering the laser source¹⁸ or by recording and incoherently combining multiple holograms after providing some type of noise decorrelation between the captured data (Multi-Look DH (MLDH) techniques)^{19–27}. Speckle decorrelation can be provided, e.g., by wavelength²⁶, polarization²⁵, illumination angle diversity²⁷, or by adopting a moving rough diffuser^{19,20} at the cost of set-up complexity. A hybrid approach that can simulate the moving diffuser action by random resampling masks has been demonstrated to be effective in reducing the additive noise²⁸. Moreover, a coherent encoding of multiple holograms, which preserves the coherence between the amplitude and phase information of the denoised complex reconstruction, has been achieved²⁹. Furthermore, the presence of turbid media made of inanimate or live microorganisms

has been recently demonstrated to be effective in providing the desired decorrelation, therefore one could take advantage of turbidity to improve image quality^{30–33}. Despite the remarkable noise reduction that has been demonstrated, all these multi-look strategies depend on the decorrelation extent between the single-look holograms (SLDHs) of the recorded time sequence and the saturation that occurs after combining a certain number of observables, therefore adding more data does not help the process^{22,25,28,30–33}. In particular, assuming that a set of L totally uncorrelated holograms could be captured, the noise reduction trend would be bounded by the ideal curve $1/\sqrt{L}$. Furthermore, in normal conditions, a hologram correlation stands, and, in most of the cases, the ML improvement factor is far from the ideal boundary value.

Meanwhile, several methods have been proposed to lower the speckle artifacts in a single-shot process; these methods can be divided into two main classes. One class operates on the hologram (that is, coherent techniques) with the advantage of preserving the coherence between the amplitude and phase information; therefore, the denoised reconstruction still possesses the features of a complex field that can be propagated back and forth for optical display purposes¹⁷. However, the coherent constraint limits the denoising performance. The second class works directly on the reconstruction in all the cases in which the optical display is not of interest (incoherent techniques). In this framework, speckle reduction can be performed working on a single hologram reconstruction^{34,35}, applying filtering-based methods aimed at decreasing the noise fluctuations and smoothing the flat homogeneous image segments while preserving the resolution and the image contrast of the edges. Of these methods, the Non Local Means (NLM) approach³⁶ and Bidimensional Empirical Mode Decomposition

¹Institute of Applied Sciences and Intelligent Systems "E. Caianiello", Italian National Research Council (ISASI-CNR), Via Campi Flegrei 34, 80078, Pozzuoli (Napoli), Italy and ²ECE Department, University of Connecticut, U-157, Storrs, Connecticut, 06269, USA

Correspondence: P Memmolo, E-mail: p.memmolo@isasi.cnr.it

Received 11 November 2015; revised 21 March 2016; accepted 27 March 2016; accepted article preview online 31 March 2016

(BEMD)³⁷ are remarkable strategies that have been proposed in image-processing contexts and only recently in DH, and show very high denoising performance. NLM introduces the concept of grouping and averaging similar image fragments located at non-neighboring positions³⁶, whereas BEMD performs an automatic sub-band decimation stage guided by speckle index indicators³⁷.

Recently, 3D Block Matching filtering (BM3D) has demonstrated very powerful denoising capabilities by means of a collaborative filtering strategy aimed at finding a signal representation with enhanced sparsity to better separate the noise components from the useful signal³⁸. This filtering has also been successfully applied to wavefront reconstructions in phase-shifting interferometry³⁹. However, this method strictly relies on the preliminary grouping step, whose performance is in turn dependent on the signal-to-noise ratio (SNR). In other words, in the absence of prior information concerning the noise statistics (non-Bayesian approaches), a low SNR can lead to incorrect grouping and can severely affect the reconstruction quality. The same problem occurs when adopting the NLM approach, making these two techniques strongly SNR-dependent.

Here, we combine the concepts of multi-look, grouping and collaborative filtering to achieve quasi noise-free DH reconstructions as demonstrated by our remarkable results. The approach we propose is referred to as MLDH-BM3D and surpasses the limits of both MLDH and BM3D. We introduce the Enhanced Grouping (EG) algorithm, which is demonstrated here to impose better working conditions for the iterative processing blocks of the collaborative sparse 3D filtering and, in turn, to increase their performance by drastically reducing the probability of incorrect grouping³⁸. On the other hand, MLDH-BM3D solves the problem of the ML improvement saturation threshold^{22,25,28,30-33} as it overcomes the theoretical improvement bound thanks to the Sparsity Enhancement Filtering (SEF) strategy. Therefore, MLDH and BM3D are demonstrated here to be complementary steps, mixing smart optical recording methods and numerical processing, and are necessary to each other to achieve near noise-free DH reconstructions. Experimental results are presented to validate the method in various hologram recording conditions, showing a significant qualitative and quantitative improvement in comparison to the most recent and well-assessed denoising techniques. First, MLDH-BM3D is applied to single-wavelength DH,

where optical ML is viable by means of a moving diffuser²⁹. Then, single exposure cases are tackled, where numerical ML²⁸ is required. Next, MLDH-BM3D is applied to multi-wavelength DH⁴⁰⁻⁴², resulting in very efficient denoising of color hologram reconstructions. In our experiment, the noise level is reduced by up to 98% in the background regions and up to 92% in the signal regions, percentages significantly higher than the current state of the art in DH, providing hologram reconstructions whose quality is comparable, in terms of SNR⁴³, to the quality achievable with non-coherent techniques.

MATERIALS AND METHODS

Working principle of MLDH-BM3D

The MLDH-BM3D algorithm consists of two main processing steps, EG and SEF, as sketched in the block diagram of Figure 1. The basic idea is to inspect the input image looking for non-adjacent image fragments (blocks) sharing a certain extent of similarity to a given reference block. EG involves a proper reconstruction of the hologram using a MLDH algorithm, followed by stacking the blocks grouped according to a certain similarity rule and providing as output the noisy groups. SEF processes together all the blocks belonging to each group following the collaborative filter paradigm^{38,44}. That is, each block cooperates to filter the entire group and denoising is performed on the stack represented in a proper 3D-transform domain taking advantage of its very sparse representation. The output of SEF is a set of near noise-free groups contributing to form the denoised hologram reconstruction, yielded after applying inverse stacking. A discussion of the role of EG and SEF is provided in the following subsections.

Enhanced grouping

Let $\{H_1, \dots, H_L\}$ be the sequence of L holograms recorded in the acquisition plane while providing some type of noise diversity, e.g., introducing a moving diffuser in a classical DH setup in the reflection configuration. After performing the numerical propagation $P_T\{\dots\}$ of each hologram at the best focus distance z , we can define the Single-Look (SL) and Multi-Look (ML) reconstructions in the focus plane as:

$$\begin{aligned} C_{SL_i} &= |P_T\{H_i; z\}| \quad i = 1, \dots, L \\ C_{ML} &= \frac{1}{L} \sum_{i=1}^L |P_T\{H_i; z\}| \end{aligned} \quad (1)$$

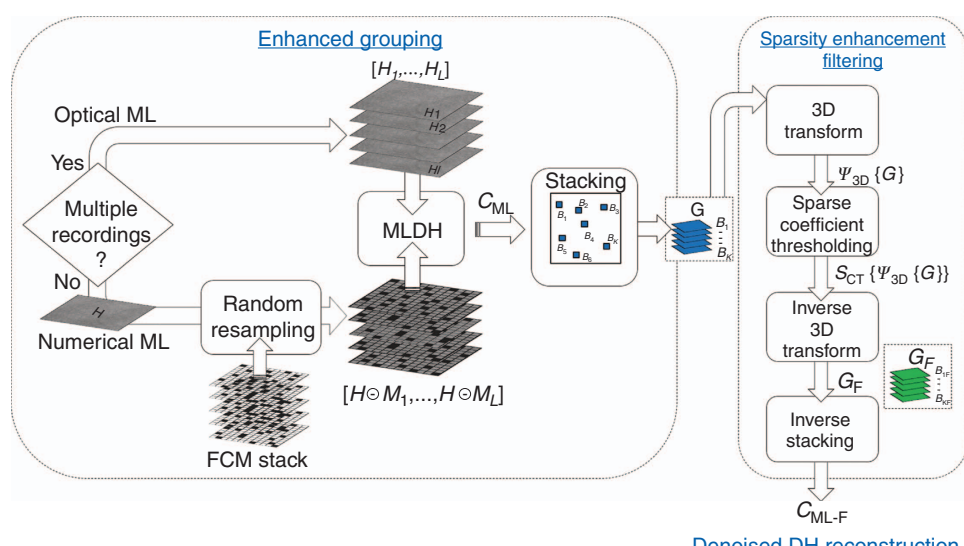


Figure 1 Block scheme of the MLDH-BM3D algorithm. EG and SEF are sequential and complementary steps returning the MLDH-BM3D reconstruction.

To evaluate the quality of such reconstructions, we introduce the percentage noise contrast, N_C , defined as

$$N_C(L) = 100 \frac{\sigma_{\text{ML}}(L)\mu_{\text{SL}}}{\sigma_{\text{SL}}\mu_{\text{ML}}(L)} \quad (2)$$

where μ_{SL} , σ_{SL} , μ_{ML} and σ_{ML} are the average values and the standard deviations of the gray level distribution in the case of SL and ML, respectively. These quantities are evaluated over homogeneous image segments, $\bar{C}_{\text{SL},i}$ and \bar{C}_{ML} , i.e., where the spatial distribution of the useful signal is expected to be flat and any fluctuation is attributed to noise. Therefore, a reduction in the percentage of noise contrast is expected as a result of the improvement in the image quality. In Equation (2), the dependency of the noise contrast on the number of looks, L , is highlighted for the sake of clarity. The estimator defined in Equation (2), is sometimes referred to as the normalized dispersion index and is widely used to quantify the performance of noise reduction methods based on the encoding of multiple holograms^{28–30,32}. By assuming uncorrelated recordings, it follows that

$$\text{VAR}[\bar{C}_{\text{SL},i}] \triangleq \sigma_{\text{SL}}^2 \quad (3)$$

$$\text{VAR}[\bar{C}_{\text{ML}}] \triangleq \sigma_{\text{ML}}^2 = \frac{\sigma_{\text{SL}}^2}{L} \quad (4)$$

where $\text{VAR}[\dots]$ indicates the variance operator. Note that by substituting Equation (4) into Equation (2) and assuming $\mu_{\text{ML}}=\mu_{\text{SL}}$ (e.g., see Refs. 15,20,22,28,29), we can evaluate the lower bound^{15,22,25,28,30–33} of $N_C(L)$ achievable by the multiple uncorrelated holograms averaging method (MLDH), which equals $100/\sqrt{L}$. In other words, acquiring and incoherently combining a set of holograms with some extent of noise uncorrelation between them results in a saturation of the improvement.

Whenever a set of nearly uncorrelated holograms is not available, this process can be synthesized by starting from one single acquisition and introducing random resampling masks in the reconstruction formula, as in Refs. 28,29. Therefore, noise diversity can be simulated and the ML observable is

$$C_{\text{ML}} = \frac{1}{L} \sum_{i=1}^L |P_T\{H \odot M_i; z\}| \quad (5)$$

where \odot denotes the element-wise product²⁸ and M_i indicates the i -th binary mask used to provide a random resampling of the hologram H . The distribution of zeros and ones in each mask is chosen according to the Fair Constrained Masking (FCM) criterion, which is described in detail in Ref. 28. After reaching the number of holograms L_{sat} corresponding to the noise contrast saturation value (which depends on the correlation coefficient between the recordings and is bound by the ideal curve), adding more data does not provide a significant improvement^{15,22,25,28,30–33}. Hence, a different method must be adopted to suppress the speckle noise in DH. Grouping is a recently proposed technique aimed at building stacks, i.e. the groups, made of image blocks similar to a given reference. Once the groups are formed, the blocks of each group are processed together using a sparsity enhancement filtering technique^{38,44}. This approach has been demonstrated to be effective; however, its performance is severely dependent on the SNR of the input observables, as will be illustrated.

Therefore, given a certain reference block B_R of $M \times M$ pixels, a block B_k belongs to the group G_R if it satisfies the following:

$$d_{L_2}(B_k, B_R) < d_T \quad (6)$$

where d_{L_2} denotes the L_2 -norm and d_T is a threshold distance. In principle, if the observables were uncorrupted by noise, the distance

of each block to the reference would be a deterministic value \bar{d} ; however, the distance of each block is instead a random variable in the non-ideal case of noisy observables. In the work by Dabov *et al.*³⁸, by considering an additive zero-mean Gaussian noise, d_{L_2} was modeled as a chi-squared random variable. If we apply the grouping step to a SL noisy hologram reconstruction following the criterion described in Equation (6), we can evaluate the statistics of the chi-squared model, described in Ref. 38:

$$\begin{aligned} E[d_{L_2}] &= \bar{d} + 2\sigma_{\text{SL}}^2 \\ \text{VAR}[d_{L_2}] &= \frac{8\sigma_{\text{SL}}^2}{M^2}(\sigma_{\text{SL}}^2 + \bar{d}) \propto \sigma_{\text{SL}}^4 \end{aligned} \quad (7)$$

where $E[\dots]$ denotes the expectation operator. Note that the variance of the distance estimator is proportional to the 4th power of the noise standard deviation. From Equation (7), the critical effect on the grouping performance of a low SNR reconstruction is apparent even in the simple case of additive noise, leading to incorrect grouping. In Ref. 38, the authors proposed coping with the incorrect grouping problem by introducing a coarse pre-filtering of the noisy observables and foreseeing the presence of two consecutive 3D filtering steps. However, in DH reconstructions, the additive model does not stand and a mixture of correlated speckle and additive noise corrupts the observables, therefore the grouping performance is expected to dramatically worsen even when adopting the coarse filtering strategy, as will be shown in the following section. Enhanced grouping is a hybrid approach combining the concepts of grouping and ML to tackle the incorrect grouping problem in DH in all cases where a set of enough uncorrelated holograms is available (see the upper processing branch in the block scheme of Figure 1) or this can be effectively simulated by randomly masking^{28,29} one acquisition (as shown in the lower branch of Figure 1). If the input observables are MLDH reconstructions, it follows that

$$\text{VAR}[d_{L_2}^{\text{ML}}] \propto \sigma_{\text{ML}}^4 = \frac{\sigma_{\text{SL}}^2}{L} \quad (8)$$

That is, the probability of incorrect grouping reduces by a factor equal to the square power of the number of holograms. Therefore, the following sparsity enhancement filtering can be applied once, reducing the speckle noise fluctuations while preserving the object features.

Sparsity enhancement filtering

SEF is a procedure that takes advantage of the previous grouping step and processes all the blocks of each group together to improve the filtering performance. If we denote a group consisting of K blocks as $G=[B_1, \dots, B_K]$, a strong correlation exists between neighbor pixels of each block and between homologous pixels. Homologous pixels are all the pixels belonging to different blocks of the group and located in the same position inside the block. Therefore, a sparsity promoting transform can provide a proper representation of the group using a few significant components, allowing for better discrimination between the useful signal coefficients and the ones related to only noise. In particular, the SEF strategy consists of three main steps to be applied to each group as described in Ref. 38 and listed as follows:

- 3D transform of the group, resulting in a sparse representation of G by a number of transform coefficients, $\psi = \gamma + \eta$, given by the sum of the number of noise components, η , and the number of components representing the useful signal, γ .
- Selection of the most representative signal components, $\psi' \cong \gamma$, by sparse coefficient thresholding.
- 3D inverse transform of the filtered sparse representation of G .

Therefore, for each group G , SEF provides its filtered version, G_F :

$$G_F = [B_{1F}, \dots, B_{KF}] = \text{SEF}\{G\} = \Psi_{3D}^{-1}\{S_{\text{CT}}\{\Psi_{3D}\{G\}\}\} \quad (9)$$

where $\Psi_{3D}\{\dots\}$ and $S_{\text{CT}}\{\dots\}$ are the 3D transform and the sparse coefficient thresholding operators, respectively, and B_{iF} ($i=1,\dots,K$) denotes the filtered version of the block B_i . Contrary to the NLM approach^{36,45}, a block B_i is allowed to belong to several groups, therefore the group dimensions are not fixed and many estimates can be obtained of the same block. The final filtered MLDH-BM3D reconstruction, referred to here as $C_{\text{ML-F}}$, is obtained by inverse stacking, $I_S[\dots]$, which involves collecting all the filtered groups, element-wise averaging the overlapping blocks and tiding up each block to the right position of the image:

$$C_{\text{ML-F}} = I_S[B_{jF}; j = 1, \dots, N_B] \quad (10)$$

where N_B is the total number of blocks. In contrast to Ref. 38, because of the enhanced grouping approach, SEF needs to be performed only once to provide a reliable estimate of the useful signal because the input observables are less noisy and the probability of incorrect grouping is drastically reduced.

Experimental set-up

The set-up adopted in our experiment is shown in Figure 2. The digital holograms are recorded in a lens-less configuration and two lasers with different wavelengths, λ , are used. The optical configuration is arranged to combine the two lasers (a He–Ne laser emitting at $\lambda = 632.8$ nm and a DPSS laser emitting at $\lambda = 532$ nm) along the same optical paths for both the reference and the object beams. The reflecting prism (RP) is placed only in the path of the red laser beam (having a shorter coherence length of approximately 30 cm with respect to the green laser, whose coherence is 80 m), permitting the matching of the optical path of the two interfering beams inside the optical coherence length of the red laser. The light scattered by the rotating diffuser (D) is used to illuminate the object (O), and a rotator (R) is used to record the object at different angles. Employing a moving diffuser has been demonstrated to provide sufficient temporal diversity between multiple speckle patterns for a MLDH strategy to

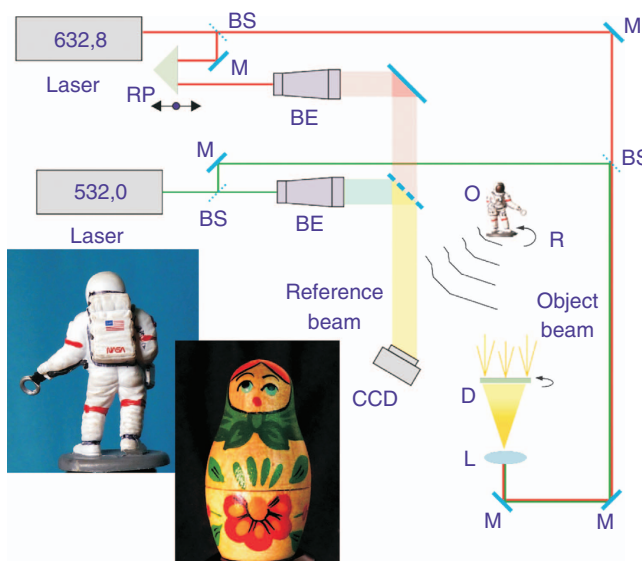


Figure 2 Optical setup for two wavelength digital hologram recordings of toy puppets. M, mirror; BS, beam splitter; BE, beam-expander; RP, reflecting prism; CCD, charge coupled device; D, rotating diffuser; R, rotator and O, object.

benefit from its use^{19,20}. When a diffuser is not available, its action needs to be properly simulated as discussed in the following section^{28,29}.

The beam that is reflected by the beam splitter (BS) impinges on the camera sensor through a couple of mirrors (M) and acts as a reference-beam. The digital holograms were acquired using a Charge Coupled Device (CCD) camera, with a resolution of 1280×1024 square pixels (with $6.7 \mu\text{m}$ pixel pitch) and an 8-bit camera depth at a distance of 85 cm from the object. The imaged field of view is approximately a 6° solid angle. To test the proposed method, we conducted four types of experiments: multiple recordings with a single-wavelength ($\lambda = 532$ nm) and activated D (R disabled); a single recording with a single wavelength ($\lambda = 532$ nm) where D and R were disabled; multiple recordings with a single-wavelength ($\lambda = 532$ nm) and activated R (D disabled) and a single recording with dual-wavelengths where D and R were disabled. The photographs in the inset of Figure 2 show two of the objects recorded, specifically an astronaut puppet 45 mm in height and 35 mm in width and a matryoshka doll 40 mm in height and 22 mm in width. Other puppets used in the reported experiments have similar sizes.

RESULTS AND DISCUSSION

Experimental validation of the optical ML

The goal of the first experiment was to demonstrate that the joint action of MLDH, grouping and collaborative sparsity enhancement filtering is capable of suppressing the mixture of speckle and additive noise in DH.

Moreover, our goal was to demonstrate that each processing block is necessary to the others and that the cascade allows the process to result in a quasi-noise free DH reconstruction. The interferometer was first adopted to acquire a set of $L = 100$ holograms of an object (a small astronaut puppet), captured while rotating D to provide speckle diversity. Each hologram was reconstructed as in Equation (1) and processed according to Equations (9) and (10). Figure 3a shows the SLDH reconstruction of the object, which was severely corrupted by the noise inherent to the coherent recording process. Due to the high noise level, both NLM and BM3D filtering applied to the SLDH images are unsuccessful because the grouping procedure fails, as apparent from Figure 3c and 3e. As a consequence of the incorrect grouping, image fragments are processed together even though they should not belong to the same class, and the result is the presence of sudden spikes and patches that corrupt the NLM and BM3D reconstructions. Therefore, the object shape is not correctly recovered at all the points of the image. However, a ML strategy yields a significant gain, as evident from the image reported in Figure 3b, showing attenuated noise in both the background and the object areas. To quantify this ML gain, the percentage noise contrast, $N_C(L)$, defined in Equation (2), was measured over the homogeneous image segments, i.e., where a smooth gray level distribution is expected and any oscillation is considered noise^{22,25,28,30–33}. Therefore, a decrease in this estimator can be obtained when L increases as a result of the ML improvement, as shown by a blue solid line in Figure 4a. After combining the $L = 100$ looks, the percentage noise contrast is lowered up to 18.3%, corresponding to a ML improvement of 81.7%. However, an improvement saturation is apparent from the plot in Figure 4a, therefore a similar result could be obtained with $L = 40$ looks, saving both acquisition and computational time. In Figure 4a, the theoretical improvement bound is also reported (see the red line), i.e., the trend achievable by combining holograms with fully uncorrelated noise. Much effort has been spent to provide noise diversity in the recording setup to obtain noise contrast values approaching this

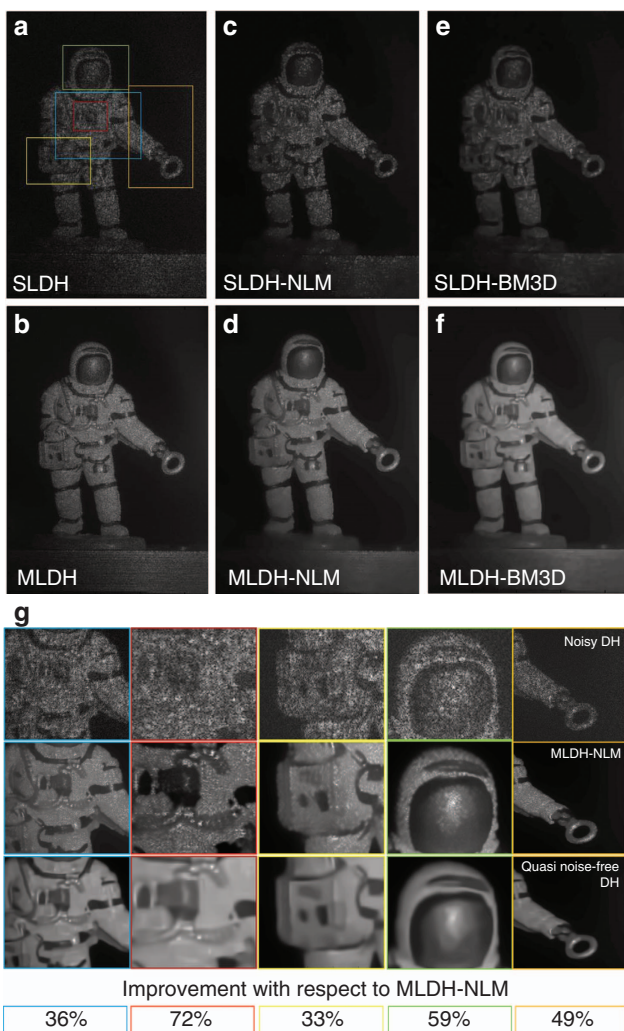


Figure 3 Comparison between noisy and denoised DH reconstructions. (a) Noisy SLDH reconstruction. (b) MLDH. (c) SLDH-NLM cascade. (d) MLDH-NLM cascade. (e) SLDH-BM3D. (f) Quasi noise-free MLDH-BM3D reconstruction. (g) Details corresponding to SLDH (top row), MLDH-NLM (middle row) and MLDH-BM3D (bottom row). The enlarged areas correspond to the color boxes in a. In the bottom panels, the calculations of the percentage noise contrast improvements of MLDH-BM3D with respect to MLDH-NLM are reported.

bound^{22,23,25}. Conversely, the proposed algorithm is able to get rid of these noise fluctuations, achieving quasi-noise free DH reconstructions and overcoming for the first time the theoretical ML improvement bound. The results of the application of the cascade EG-SEF are reported in Figure 3d and 3f, where the images obtained by MLDH-NLM and MLDH-BM3D are shown, respectively. For a better comparison, enlarged details of the images in Figure 3a, 3d and 3f corresponding to the color boxes indicated in Figure 3a, are shown in Figure 3g, where an impressive improvement is clearly appreciable with respect to the SLDH. As a result of the noise suppression, a flat gray level distribution is achieved in the smooth areas while preserving the edges. Indeed, the processing result is not a smoothing but instead a remarkable enhancement of the finer details of the object that become resolvable in the processed MLDH-BM3D reconstruction (e.g., see the blue and red boxes in Figure 3g). In this sense, NLM is found to be effective in DH when combined with ML; however, the MLDH-NLM cascade provides sub-optimal results with respect to

MLDH-BM3D. Via a direct comparison of the two methods, in terms of percentage noise contrast enhancement, we reveal an improvement up to 72% for MLDH-BM3D with respect to MLDH-NLM, as reported at the bottom of Figure 3g. We also evaluated the computational costs of the proposed technique by calculating the time-consumption of a generic MLDH-BM3D reconstruction. This process consists of L numerical reconstructions (i.e., the looks), their average operation to perform the MLDH step, and the BM3D algorithm execution, using square blocks of 8 × 8 pixels. For example, the MLDH-BM3D reconstruction in Figure 3f was obtained in 9.32 s (5.25 s for the L looks calculation, 0.85 s to compute the average value and 3.22 s for the BM3D algorithm) using a MATLAB script implemented on a Desktop PC with Intel(R) Core(TM) i7-2600 CPU @ 3.40 GHz and 32 GB of RAM.

Therefore, we chose BM3D to implement the last block of the scheme in Figure 1 and we refer to MLDH-BM3D as the denoising method providing quasi-noise free DH reconstructions. In fact, the percentage noise contrast measured over the MLDH-BM3D image decreases up to 5.6% in the case of the test area of Figure 4a (this is denoted by a yellow box in the inset), corresponding to an improvement of 94.4% and a noise standard deviation of $\sigma_{\text{MLDH-BM3D}} = 2 \times 10^{-4}$ (see Table 1), i.e., 19 times better than the value obtainable from the SLDH reconstruction. To give an indication of the object's true shape, a photo of the astronaut puppet is shown in Figure 4b. To prove the capability of MLDH-BM3D to overcome the ML improvement bound, we repeated the percentage noise contrast measures over different homogeneous segments indicated by the numbered yellow boxes, finding convincing results that are reported in Figure 4b and Table 1. The MLDH-BM3D cascade enables a jump from the allowed to the prohibited ML improvement zone, reaching up to 98% enhancement, and a standard deviation lower than 10^{-4} , enabling a yield of up to 28 times gain with respect to SLDH, values far beyond the current state of the art in DH (see columns A1-A5 in Table 1). Moreover, we measured N_C ($L=100$) over a signal region inside the object (the region corresponding to the astronaut leg, as shown in the inset of Figure 4a), and the measured improvement (see Table 1, column A6) shows the capability of the proposed strategy to suppress noise both in the background area and inside the object, i.e., where multiplicative speckle correlated to the useful signal dominates. Note that when the parameter N_C is calculated over a non-flat region, such as A6, a slightly lower improvement with respect to the other regions A1-A5 is observed due to the presence of the object's details. In other words, because the useful signal in the area being tested does not have a perfectly flat spatial distribution (rather it shows a spatial variability due to the object's details), the standard deviation of the gray level distribution is not expected to approach the null value as a result of noise mitigation. It is clear that the sole evaluation of the percentage noise contrast, defined in Equation (2), is not sufficient to assess the level of improvement in such areas. In the following, we will add to our analysis a further improvement measure, directly showing the relative deviation of the gray level distribution in two signal regions of a color DH. Remarkably, the quality of the hologram reconstructions provided by MLDH-BM3D is comparable to that achievable using non-coherent techniques. In Ref. 43, it was demonstrated that the noise level in the case of incoherent imaging is approximately one order of magnitude lower than the noise level obtained using a coherent source. We achieved this goal, as highlighted in the last row of Table 1, where the noise level for single wavelength MLDH-BM3D is at least 7.39 times better than the classical DH reconstructions.

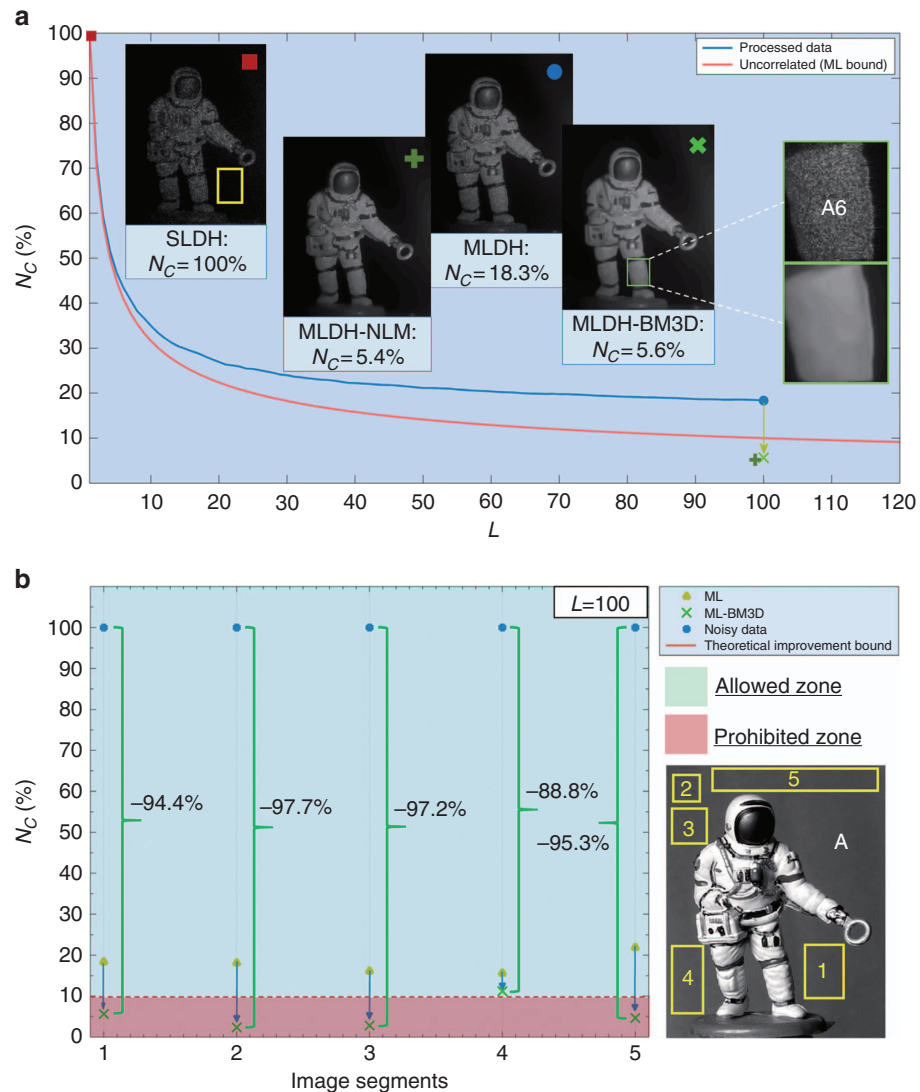


Figure 4 Quantitative evaluation of the algorithm performance. (a) N_C (%) vs. the number of looks, L , in the MLDH image (blue line), showing a ML improvement saturation. The theoretical ML improvement bound is plotted with a red line. The N_C values corresponding to $L=100$ for MLDH, MLDH-NLM and MLDH-BM3D are indicated with a blue circle, an orange plus sign and a green cross, respectively. The plot shows the noise reduction percentage with respect to the noise level of the SLDH image (indicated by a red square). (b) N_C (%) measured over the image segments A1-A5 of the SLDH (blue circles), MLDH (yellow triangles) and MLDH-BM3D (green crosses). The cascade of EG and SEF allows the theoretical ML improvement bound to be overcome and quasi noise-free DH reconstructions to be obtained.

Numerical ML: application to single-shot hologram recordings

Whenever multiple holograms are available, the MLDH-BM3D approach has proved to be effective at the cost of recording complexity. However, in many cases there is no possibility of performing an optical ML for denoising purposes. Therefore, we conducted different experiments to examine the case of single-shot hologram recording, i.e., when optical diversity between the speckle patterns cannot be provided and one single hologram needs to be denoised. Figure 5 shows the results of the application of MLDH-BM3D with numerical ML performed using the encoding formula in Equation (5). Following the FCM strategy²⁸, we built 10 binary re-sampling masks corresponding to $L=10$ numerical looks. The decrease in the percentage noise contrast by means of numerical ML is shown in Figure 5 along with the SLDH and MLDH images of the object (a toy car hologram was captured for the scope). As expected, an appreciable improvement is provided by FCM and the percentage noise contrast decreases by up to

36.9% (i.e., a 63.1% gain), close to the theoretical bound value. The noise contrast is measured over the expected flat area indicated by the yellow box in Figure 5. However, the performance is worse than that achievable by optical diversity. Nonetheless, the application of the EG-SEF cascade yields a noise contrast decrease of 94.2%, corresponding to a standard deviation value $\sigma_{\text{MLDH-BM3D}} = 3 \times 10^{-4}$. The gain is easily visible in the corresponding reconstruction shown in the inset, where the overall image contrast is dramatically improved, as is the flatness over homogeneous areas. Owing to the possibility of performing single-shot recordings, it is easier and less time consuming to acquire holograms from different view angles of an object by automatically rotating it to collect 3D information. Therefore, we acquired and processed holograms of different astronaut puppets while rotating them by one-degree steps, as sketched in Figures 6a and 2. Numerical ML was performed for each hologram of the sequence to build up quasi-noise free holographic movies of the rotating objects, as

Table 1 Quantitative performance evaluation

	Optical ML, $L = 100$						Numerical ML, $L = 10$							
	A1	A2	A3	A4	A5	A6	B	C	D	E	F	G	H	I
(100- N_C) (%)	94.37	97.66	97.17	88.79	95.34	85.95	94.19	94.65	93.35	94.91	62.39	63.75	66.61	80.22
σ_{SL}	0.0038	0.0025	0.0025	0.0022	0.0028	0.0451	0.0032	0.0039	0.0095	0.0031	0.0138	0.0118	0.0049	0.0638
σ_{ML}	0.0007	0.0005	0.0004	0.0004	0.0006	0.0252	0.0018	0.0027	0.0059	0.0023	0.0109	0.0098	0.0030	0.0075
$\sigma_{MLDH-BM3D}$	0.0002	0.0001	0.0001	0.0002	0.0001	0.0061	0.0003	0.0005	0.0009	0.0004	0.0051	0.0041	0.0020	0.0015
$\sigma_{SL}/\sigma_{MLDH-BM3D}$	19.00	25.00	25.00	11.00	28.00	7.39	10.67	7.8	10.56	7.75	2.71	2.88	2.45	42.53

Measures carried out over flat regions inside the object are highlighted in the green rectangle. Some of the most remarkable outcomes are highlighted in red.

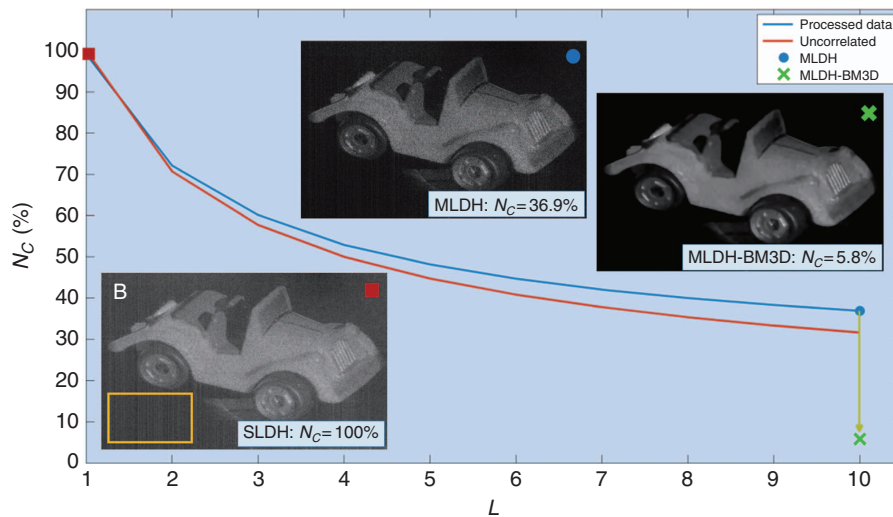


Figure 5 N_C (%) vs. L (blue solid line). Measures indicate the case of single-shot recording, followed by numerical ML performed using the FCM masking method²². The theoretical ML improvement bound is plotted with a red line. N_C is calculated in the region indicated by the yellow box in the inset.

shown in Supplementary Movies 1–3 where a comparison between the SLDH and MLDH-BM3D reconstructions is shown in the color boxes. Frames and enlarged details extracted from the movies are shown in Figure 6b–6e, where an impressive processing gain is apparent in both the flat areas and the boundaries. The noise suppression in the MLDH-BM3D movies allows an appreciation of the changes in reflectivity in some object areas (e.g., see the reconstruction of the object rotated by 270° in Figure 6c and Supplementary Movie 2, or the reconstructions of Figure 6e and the corresponding enlarged details of the astronaut leg and backpack, shown in Supplementary Movie 1), with light reflecting differently due to the object's rotation. In Figure 6c (no rotation) and the corresponding enlarged image showing the astronaut's chest, the proposed filtering strategy allowed the recovery of details of the puppet's belt that were not at all evident in the corresponding noisy DH image (Figure 6b). Indeed, even in the case of numerical ML, noise reduction does not correspond to a smoothing of the image boundaries but rather to a visible contrast enhancement, and only the homogeneous image areas are made flatter. To demonstrate this property, we measured the image contrast along a line crossing the narrow stripes of the US flag depicted on the backpack of the puppet in Figure 7a and 7b. The images in Figure 7a and 7b are frames extracted from Supplementary Movie 3. Figure 7c shows a comparison between the contrast of the noisy SLDH (red line) and the denoised MLDH-BM3D reconstruction (green line). Noise suppression not only is obtained without sacrificing the resolution of the unprocessed image but also results in a significant contrast

improvement, making all seven stripes resolved and more visible. Notably, the noise reduction does not allow for an enhancement in the resolution of the optical system beyond the diffraction limit or the limit imposed by the geometrical resolution to be overcome but an improvement in only the noise equivalent resolution, defined as in Ref. 46. In other words, the details recovered as a result of noise mitigation, e.g., in Figures 3b and 7, correspond to spatial frequencies that were also collected by the optical system in the case of SLDH reconstructions, but were lost due to noise fluctuations corrupting the images. The values of N_C ($L=10$) and σ obtained in these cases are reported in Table 1 (columns C–E) where some of the most remarkable outcomes are highlighted in red.

MLDH-BM3D for multi-wavelength DH

We report the results of the last set of experiments to demonstrate the applicability of the method to color holography. In these experiments, lasers at $\lambda = 532$ nm and $\lambda = 632.8$ nm were used to capture the green and red components of the illuminated object, respectively. The holograms corresponding to the two components were separately processed as in Equations (5), (9) and (10), then they were properly matched^{11,41} using the Spatial Correlation Coefficient (SCC) maximization approach proposed in Ref. 41, and the denoised color MLDH-BM3D was synthesized. Note that the effectiveness of the matching of the SCC based method is strongly dependent on the noise level and the finite resolution of the employed sensor (i.e., the finite size of the CCD pixel). Therefore, the MLDH-BM3D reconstructions

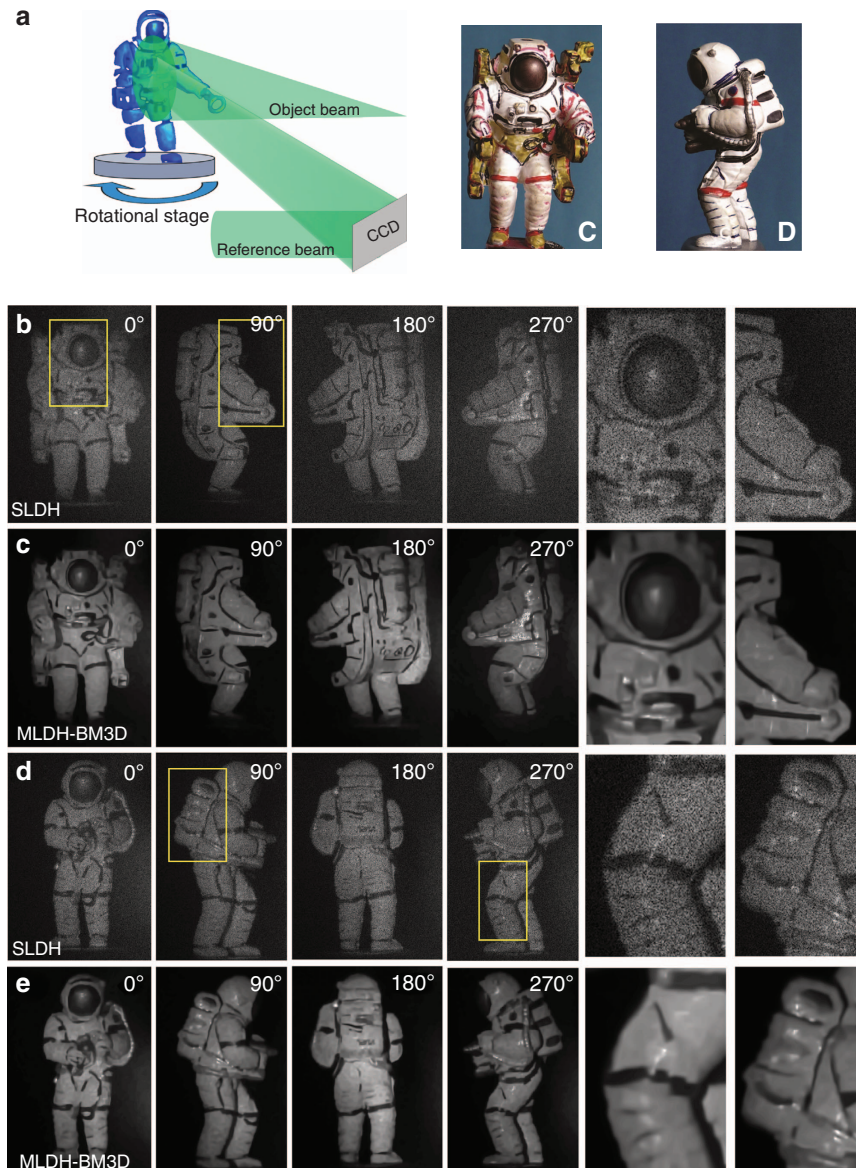


Figure 6 (Supplementary Movies 1 and 2). Numerical MLDH-BM3D is applied to objects rotated by means of a stage, as sketched in (a) along with the corresponding photos. (b, d) SLDH. (c, e) MLDH-BM3D reconstructions. Details of the image segments indicated by yellow boxes are shown on the right side of the panel. As a result of denoising, MLDH-BM3D reconstructions show finer details, are better resolved and have improved sharpness on the edges and flatness over the homogeneous segments. Images in b, c are frames extracted from Supplementary Movie 2. Images in d, e are extracted from Supplementary Movie 1.

obtained by processing each component of the color hologram provide better spatial matching once the RGB reconstruction is synthesized. In Figure 8, we show the results of the MLDH-BM3D denoising process separately applied to the noisy green and red holograms of a matryoshka doll. The noisy SLDH reconstructions are shown in Figure 8a and 8c for the green and red components, respectively. The corresponding denoised MLDH-BM3D reconstructions are reported in Figure 8b (green component) and Figure 8d (red component), showing an apparent enhancement in the image quality in both the background and the signal region. In this case, we first evaluated the performance of the proposed method by calculating the percentage noise contrast improvement over the background regions (yellow boxes). Remarkably, we found improvements of 91.68% and 90.23% for the green and red reconstructions, respectively. Moreover,

two quasi-flat signal regions (blue boxes) were tested, resulting in improvements of 92.11% (green) and 85.71% (red). To highlight the impressive gain in the noise suppression while preserving the edges, two regions of the puppet with several details were processed by calculating their relative deviation (R_D) distributions²⁸. These regions are shown in Figure 8e and 8f, as functions of the pixel coordinates, (j, k) , inside each region for the SLDH and MLDH-BM3D reconstructions, respectively. In particular, $R_D(j, k)$, calculated over the region of the SLDH green component (green box in Figure 8a), is compared with the corresponding distribution calculated over the same area of the MLDH-BM3D reconstruction. Similarly, we compared the SLDH and MLDH-BM3D red reconstructions by directly showing their relative deviations over the region indicated by the red box in Figure 8c. The pseudo-color representations of Figure 8e show the

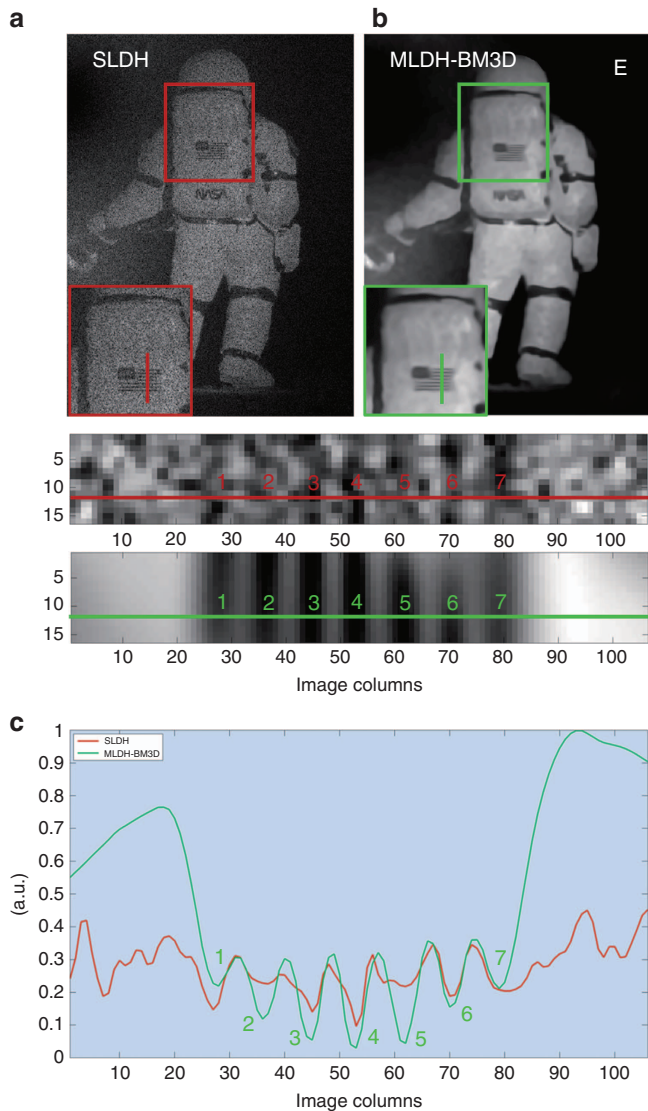


Figure 7 (Supplementary Movie 3) Contrast analysis. **(a)** SLDH. **(b)** MLDH-BM3D. **(c)** Image contrast plotted along the lines indicated in the insets of **a** and **b**. Red: SLDH. Green: MLDH-BM3D. A close up of the flag stripes is also shown, demonstrating the capability of MLDH-BM3D to resolve all seven stripes on the US flag.

detrimental effect of noise corrupting each component with sudden unwanted spikes randomly distributed over the areas tested. However, for both of the selected regions, a direct inspection of Figure 8e and 8f shows an evident denoising gain as the distributions of $R_D(j, k)$ in Figure 8f exhibit an impressive image contrast enhancement, with sharper edges and a smoother trend over the flat areas. The color MLDH-BM3D reconstructions of the four puppets were obtained after SCC-based color matching, shown in Figure 9. In particular, Figure 9a, c, e and g show the noisy SLDH dual color synthesis. As expected, both speckle and additive artifacts severely corrupt these images. However, a remarkable processing gain is achievable, which is evident in the corresponding MLDH-BM3D dual color reconstructions in Figure 9b, 9d, 9f and 9h. Details of the image segments indicated by white boxes are reported on the right side of the panel, showing remarkable noise suppression and preservation of the fine details. A grayscale synthesis of the color reconstructions was performed as in Ref. 41 to quantitatively evaluate the achieved improvement factor.

The results are reported in Table 1 (columns F–I). In particular, in the case of the holograms (F–H), the standard deviation and the percentage noise contrast were evaluated over the homogeneous segments of the grayscale synthesis (similar to the noise measures shown previously). Again, $\sigma_{MLDH-BM3D} \approx 10^{-3}$ is obtained as a processing result. The comparison between SLDH and MLDH-BM3D in Figure 9c–f shows dual-wavelength DH reconstructions of a Pinocchio puppet and a matryoshka, where the automatic matching between the two components also improves as a result of noise suppression and a better color rendering is achieved (e.g., see the detail of the Pinocchio face on the right side of the panel). As a final performance evaluation, the percentage noise contrast was measured over a supposed flat area inside the object, which is indicated by the black box in Figure 9h.

Our aim was to quantitatively prove that the numerical MLDH-BM3D gain not only was related to additive noise suppression in the background but also involved a dramatic speckle noise reduction inside the signal region. The last column (column I) of Table 1 shows the results of this performance evaluation. Despite a single-shot recording that was performed for each of the two wavelengths (i.e., optical ML exploiting multiple recordings was not feasible), the EG-SEF strategy with numerical ML provided excellent results. Indeed, the noise standard deviation dropped from $\sigma_{SL} = 0,0638$ to $\sigma_{MLDH-BM3D} = 0,0015$, i.e., an improvement of 42.5 times. Such impressive values are far beyond the current state of the art in DH and the MLDH-BM3D reconstruction quality here becomes for the first time comparable to non-coherent imaging. However, it is important to note the improvements in the percentage noise contrast for the cases F, G and H in Table 1 are low compared with the results achieved for the separated color components, as shown in Figure 8. This improvement loss is caused by SCC color matching due to its heavy dependency on the finite resolution of the employed sensor.

CONCLUSIONS

The coherent nature of the laser sources employed in the DH recordings is the inherent cause of the image degradation due to the mixture of multiplicative speckle and additive Gaussian noise. As a consequence, a DH reconstruction may be much worse than a standard photograph of an object, therefore it is less able to represent finer details and sharp boundaries, as well as the flatness of homogeneous areas. To tackle the noise problem in DH, a variety of non-Bayesian approaches have been preferred^{47,48} as they do not rely on prior information concerning the noise statistics. Whenever multiple hologram recordings are available with uncorrelated noise, MLDH is effective in reducing the noise level in flat regions while preserving the resolution of the unprocessed reconstruction^{22,25,28,30–33}. In addition, MLDH can be performed on a single-shot hologram capture by simulating the action of a rough moving diffuser (i.e., noise diversity) via random resampling masks^{28,29}. However, a theoretical ML improvement bound exists, which limits the performance of MLDH even in the ideal case of fully uncorrelated noise. A different and very effective approach to suppress additive noise in the wider research field of image processing is based on the concept of grouping. This approach involves stacking and processing together non-neighboring fragments of the image that share a certain extent of similarity to a given reference according to a chosen similarity rule³⁶. If the groups are processed following a sparsity promoting filtering based on a 3D transform, remarkable noise reduction is achievable³⁸. However, the performance of these filters is strongly dependent on the input noise level and, in the case of DH recordings, severe noise degradation leads to incorrect grouping.

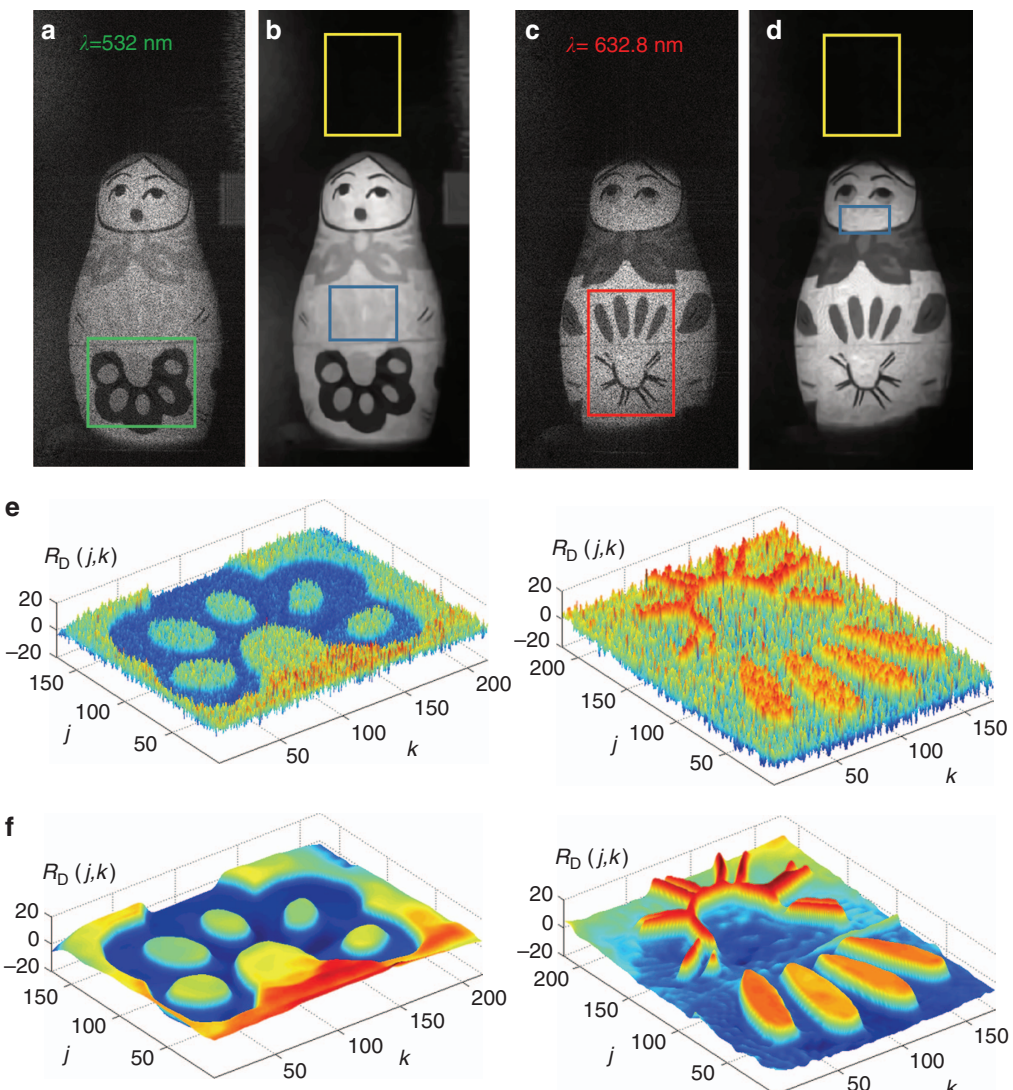


Figure 8 Numerical MLDH-BM3D applied to color holograms (green and red) of a matryoshka doll. **(a, c)** SLDH. **(b, d)** MLDH-BM3D. **(e)** Relative deviation (R_D) visualization of selected details on the object highlighted by green and red boxes in **a** and **c**, respectively. **(f)** The same regions extracted from MLDH-BM3D reconstructions in **b** and **d** for a direct comparison. Yellow and blue boxes in **b** and **d** identify background regions and signal regions, respectively, over which the percentage image contrast is evaluated.

Moreover, these filters are not optimized to suppress the mixture of additive and multiplicative noise, such as speckle artifacts, that are not an issue in incoherent imaging. Therefore, such filters cannot properly reconstruct the object features in a DH reconstruction.

In this work, we proposed a de-noising strategy that mixes smart DH recordings and numerical processing to overcome the ML improvement limit and solve the incorrect grouping problem. The algorithm is made of two steps, EG and SEF. EG uses a MLDH strategy as a pre-filtering step to reduce the noise contrast to a value close to the theoretical bound. This strategy works in both the case of multiple recordings (optical ML) and the case of single-shot data capture (numerical ML). SEF processes together the elements of each group and, taking advantage of a correct grouping, allows the ML improvement bound to be overcome. We call this strategy, specifically suitable for DH, MLDH-BM3D. This benefits from all the useful features of both the main processing blocks; however, EG and SEF cooperate to surpass their respective drawbacks. As a result, quasi noise-free DH reconstructions can be obtained for the first time.

Several experiments have been carried out to show the effectiveness of the method in the case of multiple DH acquisitions where optical ML is feasible. Qualitative evaluation and quantitative noise contrast measures show a remarkable improvement in reconstruction quality, far beyond the current state of the art in DH. Indeed, the percentage noise contrast improves up to 98%, with a residual noise standard deviation on the order of 10^{-4} (see Table 1). This improvement is apparent in a qualitative inspection of the images as the flatness of the homogeneous segments improves both in the background and the signal region while preserving the sharpness on the boundaries. It is of note that the noise suppression does not result in a smoothing, instead an image contrast enhancement is achieved revealing finer object details that were not evident in the noisy images (e.g., see Figure 3g), as discussed above. Next, we addressed the case of single-shot recordings, showing that the numerical MLDH-BM3D is as effective as the optical one. Again, it is possible to exceed the ML improvement bound and to obtain residual noise levels on the order of 10^{-4} . The method's capability to enhance the contrast of the useful signal as a

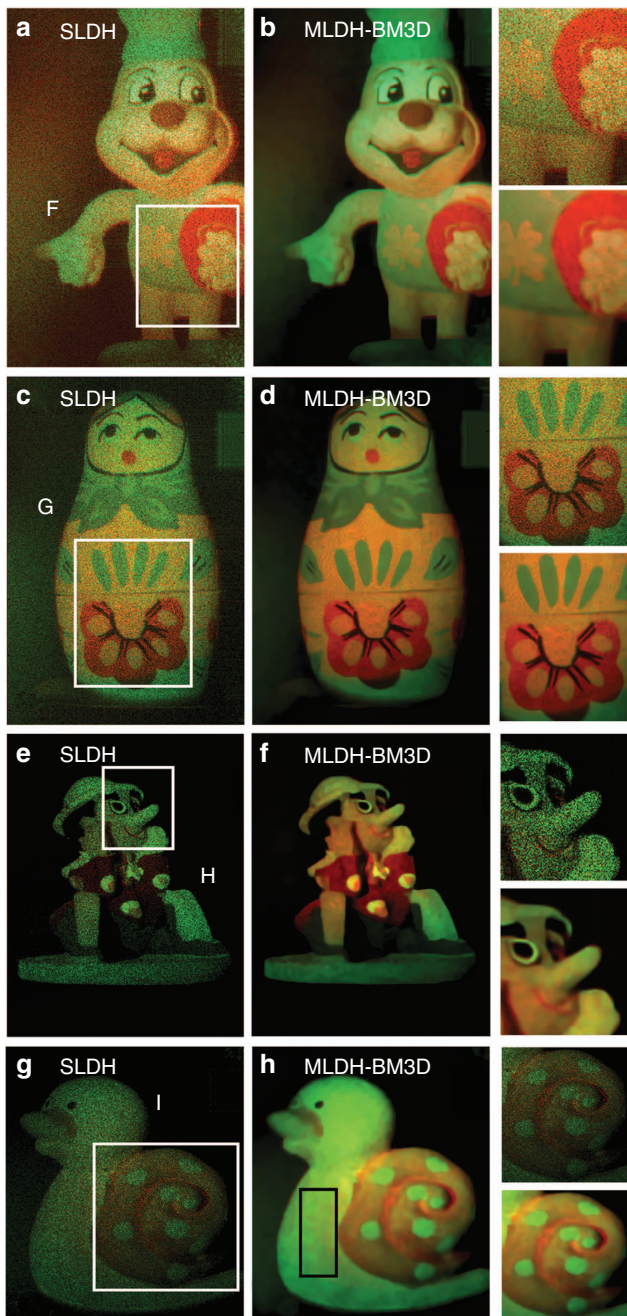


Figure 9 Dual wavelength DH. (a, c, e, g) color SLDH. (b, d, f, h) color MLDH-BM3D. Details of the image segments indicated by the white boxes are shown on the right side of the panel. The black box in h indicates the signal region where the noise measurements reported in column I of Table 1 were performed.

denoising result was also proved (see Figure 7). As a final benchmark, examples of an application of MLDH-BM3D to dual-wavelength DH recordings was reported showing denoised color reconstructions whose quality was for the first time comparable to low-coherence techniques.

ACKNOWLEDGEMENTS

This work was supported by DATABENC_Progetto SNECS-PON03PE_00163_1 Social Network delle Entità dei Centri Storici.

- 1 Osten W, Faridian A, Gao P, Körner K, Naik D et al. Recent advances in digital holography. *Appl Opt* 2014; **53**: G44–G63.
- 2 Memmolo P, Bianco V, Merola F, Miccio L, Paturzo M et al. Breakthroughs in photonics 2013: holographic imaging. *IEEE Photon J* 2014; **6**: 701106.
- 3 Cotte Y, Toy F, Jourdain P, Pavillon N, Boss D et al. Marker-free phase nanoscopy. *Nat Photonics* 2013; **7**: 113–117.
- 4 Merola F, Memmolo P, Miccio L, Bianco V, Paturzo M et al. Diagnostic tools for lab-on-chip applications based on coherent imaging microscopy. *Proc IEEE* 2015; **103**: 192–204.
- 5 Girshovitz P, Shaked NT. Doubling the field-of-view in off-axis low-coherence interferometric imaging. *Light Sci Appl* 2014; **3**: e151, doi:10.1038/lsa.2014.32.
- 6 Luo W, Greenbaum A, Zhang YB, Ozcan A. Synthetic aperture-based on-chip microscopy. *Light Sci Appl* 2015; **4**: e261, doi:10.1038/lsa.2015.34.
- 7 Bishara W, Zhu HY, Ozcan A. Holographic opto-fluidic microscopy. *Opt Express* 2010; **18**: 27499–27510.
- 8 Sobieranski AC, Inci F, Tekin HC, Yuksekaya M, Comunello E et al. Portable lensless wide-field microscopy imaging platform based on digital in-line holography and multi-frame pixel super-resolution. *Light Sci Appl* 2015; **4**: e346, doi:10.1038/lsa.2015.119.
- 9 Paturzo M, Memmolo P, Finizio A, Näslund R, Naughton TJ et al. Synthesis and display of dynamic holographic 3D scenes with real-world objects. *Opt. Express* 2010; **18**: 8806–8815.
- 10 Geng J. Three-dimensional display technologies. *Adv Opt Photon* 2013; **5**: 456–535.
- 11 Zhang ZC, You Z, Chu DP. Fundamentals of phase-only liquid crystal on silicon (LCOS) devices. *Light Sci Appl* 2014; **3**: e213, doi:10.1038/lsa.2014.94.
- 12 Shrestha PK, Chun YT, Chu DP. A high-resolution optically addressed spatial light modulator based on ZnO nanoparticles. *Light Sci Appl* 2015; **4**: e259, doi:10.1038/lsa.2015.32.
- 13 Georges MP, Vandervliet JF, Thizy C, Stockman Y, Queeckers P et al. Digital holographic interferometry with CO₂ lasers and diffused illumination applied to large space reflector metrology. *Appl Opt* 2013; **52**: A102–A116.
- 14 Chen W, Javidi B, Chen XD. Advances in optical security systems. *Adv Opt Photon* 2014; **6**: 120–155.
- 15 Locatelli M, Pugliese E, Paturzo M, Bianco V, Finizio A et al. Imaging live humans through smoke and flames using far-infrared digital holography. *Opt Express* 2013; **21**: 5379–5390.
- 16 Bianco V, Paturzo M, Finizio A, Stetson KA, Ferraro P. Portable IR laser system for real-time display of alive people in fire scenes. *J Display Technol* 2015; **11**: 834–838.
- 17 Memmolo P, Esnaola I, Finizio A, Paturzo M, Ferraro P et al. SPADEDH: a sparsity-based denoising method of digital holograms without knowing the noise statistics. *Opt Express* 2012; **20**: 17250–17257.
- 18 Redding B, Choma MA, Cao H. Speckle-free laser imaging using random laser illumination. *Nat Photonics* 2012; **6**: 355–359.
- 19 Kuratomi Y, Sekiya K, Satoh H, Tomiyama T, Kawakami T et al. Speckle reduction mechanism in laser rear projection displays using a small moving diffuser. *J Opt Soc Am A* 2010; **27**: 1812–1817.
- 20 Kubota S, Goodman JW. Very efficient speckle contrast reduction realized by moving diffuser device. *Appl Opt* 2010; **49**: 4385–4391.
- 21 Pan F, Xiao W, Liu S, Wang FJ, Rong L et al. Coherent noise reduction in digital holographic phase contrast microscopy by slightly shifting object. *Opt Express* 2011; **19**: 3862–3869.
- 22 Baumbach T, Kolenović E, Kebbel V, Jüptner W. Improvement of accuracy in digital holography by use of multiple holograms. *Appl Opt* 2006; **45**: 6077–6085.
- 23 Quan CG, Kang X, Tay CJ. Speckle noise reduction in digital holography by multiple holograms. *Opt Eng* 2007; **46**: 115801.
- 24 Leo M, Distante C, Paturzo M, Memmolo P, Locatelli M et al. Automatic digital hologram denoising by spatiotemporal analysis of pixel-wise statistics. *J Display Technol* 2013; **9**: 904–909.
- 25 Rong L, Xiao W, Pan F, Liu S, Li R. Speckle noise reduction in digital holography by use of multiple polarization holograms. *Chin Opt Lett* 2010; **8**: 653–655.
- 26 Jiang HZ, Zhao JL, Di JL. Digital color holographic recording and reconstruction using synthetic aperture and multiple reference waves. *Opt Commun* 2012; **285**: 3046–3049.
- 27 Pandey N, Hennelly B. Memory efficient noise reduction in in-line Fresnel digital holography. In: Hrabovský M, Miler M, Sheridan JT, editors. *Proceedings of SPIE Holography: Advances and Modern Trends II*. Prague, Czech Republic: SPIE. 2011; 8074: 807404.
- 28 Bianco V, Paturzo M, Memmolo P, Finizio A, Ferraro P et al. Random resampling masks: a non-Bayesian one-shot strategy for noise reduction in digital holography. *Opt Lett* 2013; **38**: 619–621.
- 29 Memmolo P, Bianco V, Paturzo M, Javidi B, Netti PA et al. Encoding multiple holograms for speckle-noise reduction in optical display. *Opt Express* 2014; **22**: 25768–25775.
- 30 Bianco V, Paturzo M, Finizio A, Balduzzi D, Puglisi R et al. Clear coherent imaging in turbid microfluidics by multiple holographic acquisitions. *Opt Lett* 2012; **37**: 4212–4214.
- 31 Bianco V, Merola F, Miccio L, Memmolo P, Gennari O et al. Imaging adherent cells in the microfluidic channel hidden by flowing RBCs as occluding objects by a holographic method. *Lab Chip* 2014; **14**: 2499–2504.
- 32 Bianco V, Paturzo M, Finizio A, Calabriga A, Javidi B et al. Clear microfluidics imaging through flowing blood by digital holography. *IEEE J Sel Top Quantum Electron* 2014; **20**: 6801507.

- 33 Bianco V, Marchesano V, Finizio A, Paturzo M, Ferraro P. Self-propelling bacteria mimic coherent light decorrelation. *Opt Express* 2015; **23**: 9388–9396.
- 34 Maycock J, Hennelly BM, McDonald JB, Frauel Y, Castro A et al. Reduction of speckle in digital holography by discrete Fourier filtering. *J Opt Soc Am A* 2007; **24**: 1617–1622.
- 35 Garcia-Sucerquia J, Ramirez JAH, Prieto DV. Reduction of speckle noise in digital holography by using digital image processing. *Optik* 2005; **116**: 44–48.
- 36 Uzan A, Rivenson Y, Stern A. Speckle denoising in digital holography by nonlocal means filtering. *Appl Opt* 2013; **52**: A195–A200.
- 37 Leo M, Piccolo R, Distante C, Memmolo P, Paturzo M et al. Multilevel bidimensional empirical mode decomposition: a new speckle reduction method in digital holography. *Opt Eng* 2014; **53**: 112314.
- 38 Dabov K, Foi A, Katkovnik V, Egiazarian K. Image denoising by sparse 3D transform-domain collaborative filtering. *IEEE Trans Image Proc* 2007; **16**: 2080–2095.
- 39 Katkovnik V, Bioucas-Dias J. Wavefront reconstruction in phase-shifting interferometry via sparse coding of amplitude and absolute phase. *J Opt Soc Am A* 2014; **31**: 1801–1810.
- 40 Zhao JL, Jiang HZ, Di JL. Recording and reconstruction of a color holographic image by using digital lensless Fourier transform holography. *Opt Express* 2008; **16**: 2514–2519.
- 41 Memmolo P, Finizio A, Paturzo M, Ferraro P, Javidi B. Multi-wavelengths digital holography: reconstruction, synthesis and display of holograms using adaptive transformation. *Opt Lett* 2012; **37**: 1445–1447.
- 42 Leclercq M, Picart P. Method for chromatic error compensation in digital color holographic imaging. *Opt Express* 2013; **21**: 26456–26467.
- 43 Bhaduri B, Tangella K, Popescu G. Fourier phase microscopy with white light. *Biomed Opt Express* 2013; **4**: 1434–1441.
- 44 Dabov K, Foi A, Katkovnik V, Egiazarian K. Image denoising with block-matching and 3D filteringIn: *Proceedings of the SPIE Electronic Imaging: Algorithms and Systems V*. San Jose, CA, USA: SPIE. 2006; 6064: 606414.
- 45 Buades A, Coll B, Morel JM. A review of image denoising algorithms, with a new one. *Multiscale Model Simul* 2005; **4**: 490–530.
- 46 Zalevsky Z, Mendlovic D. The concept of superresolution. In: *Optical Superresolution*, Chap. 3, New York: Springer. 2012; **91**: 21–23.
- 47 Rivenson Y, Stern A, Javidi B. Overview of compressive sensing techniques applied in holography. *App Opt* 2013; **52**: A423–A432.
- 48 Rivenson Y, Stern A, Javidi B. Compressive Fresnel Holography. *IEEE J Display Technol* 2010; **6**: 506–509.



This work is licensed under a Creative Commons Attribution-NonCommercial-NoDerivs 4.0 International License. The images or other third party material in this article are included in the article's Creative Commons license, unless indicated otherwise in the credit line; if the material is not included under the Creative Commons license, users will need to obtain permission from the license holder to reproduce the material. To view a copy of this license, visit <http://creativecommons.org/licenses/by-nc-nd/4.0/>

Supplementary Information for this article can be found on the *Light: Science & Applications*' website (<http://www.nature.com/lsa>).